

Exploring Hydrodynamic Closures for the Lid-driven Micro-cavity

By S. Ansumali¹, C. E. Frouzakis¹, I. V. Karlin¹
and I. G. Kevrekidis²

¹Aerothermochemistry and Combustion Systems Laboratory, Swiss Federal Institute of Technology Zurich (ETHZ), 8092 Zürich, Switzerland

²Department of Chemical Engineering, Princeton University, NJ 08544-5263, USA

(Received 31 October 2018)

A minimal kinetic model is used to study analytically and numerically flows at a micrometer scale. Using the lid-driven microcavity as an illustrative example, the interplay between kinetics and hydrodynamics is quantitatively visualized. The validity of various theories of non-equilibrium thermodynamics of flowing systems is tested in this nontrivial microflow.

1. Introduction

Flows in microdevices constitute an emerging application field of fluid dynamics (Beskok & Karniadakis 2001). Despite impressive experimental progress, theoretical understanding of microflows remains incomplete. For example, even though microflows are highly subsonic, the assumption of incompressible fluid motion is often questionable (see, e. g. Zheng *et al.* (2002)). Interactions between the relaxation of density variations, the rarefaction and the flow geometry are not completely understood. One of the reasons for this is the lack of commonly accepted models for efficient simulations of microflows.

In principle, microflows can be studied using molecular level methods, such as the Direct Simulation Monte Carlo (DSMC) method (Bird 1994). However, molecular dynamics methods face severe limitations for subsonic flows. The number of particles required for simulations in realistic geometries with large aspect ratios and the number of time steps needed to reach the statistical steady state are prohibitively high (Oran *et al.* 1998) (the time step of DSMC is $\sim 10^{-10}$ sec, while relevant physical time-scales are $\sim 10 - 100$ sec). Moreover, a detailed microscopic description in terms of the particle distribution function is not necessary for design/engineering purposes. Thus, development of reduced models enabling efficient simulations is an important issue.

In this paper we consider a two-dimensional minimal kinetic model with nine discrete velocities (Karlin *et al.* 1999; Ansumali *et al.* 2003). It has been recently shown by several groups (Ansumali & Karlin 2002*b*; Ansumali *et al.* 2004; Niu *et al.* 2003; Succi & Sbragaglia 2004) that this model compares well with analytical results of kinetic theory (Cercignani 1975) in simple flow geometries (channel flows), as well as with molecular dynamics simulations. The focus of this paper is the validation of several theoretical models of (extended) hydrodynamics versus direct numerical simulation in a non-trivial flow. For that purpose, we considered the flow in a lid-driven cavity. We will visualize the onset of the hydrodynamic description, the effect of the boundaries etc.

The paper is organized as follows: For completeness, the kinetic model (Karlin *et al.* 1999; Ansumali *et al.* 2003) is briefly presented in section 2. In section 3, we show the

relation of our model to the well-known Grad moment system derived from the Boltzmann kinetic equation (Grad 1949). We compare analytically the dispersion relation for the present model and the Grad moment system. This comparison reveals that the kinetic model of section 2 is a superset of Grad's moment system. In section 4, a parametric numerical study of the flow in a micro-cavity is presented. Results are also compared to a DSMC simulation. In section 5, the reduced description of the model kinetic equation is investigated, and a visual representation quantifying the onset and breakdown of the hydrodynamics is discussed. We conclude in section 6 with a spectral analysis of the steady state flow and some suggestions for further research (Theodoropoulos *et al.* 2000, 2004; Kevrekidis *et al.* 2003, 2004).

2. Minimal kinetic model

We consider the discrete velocity model with the following set of nine discrete velocities:

$$\mathbf{c}_x = [0, 1, 0, -1, 0, 1, -1, -1, 1], \quad \mathbf{c}_y = [0, 0, 1, 0, -1, 1, 1, -1, -1]. \quad (2.1)$$

The local hydrodynamic fields are defined in terms of the discrete population, f_i , as:

$$\sum_{i=1}^9 f_i \{1, c_{xi}, c_{yi}\} = \{\rho, j_x, j_y\}, \quad (2.2)$$

where ρ is the local mass density, and j_α is the local momentum density of the model. The populations $f_i \equiv f(\mathbf{x}, \mathbf{c}_i, t)$ are functions of the discrete velocity \mathbf{c}_i , position \mathbf{x} and time t . We consider the following kinetic equation for the populations (the Bhatnagar-Gross-Krook single relaxation time model):

$$\partial_t f_i + \mathbf{c}_i \cdot \partial_{\mathbf{x}} f_i = -\frac{1}{\tau} (f_i - f_i^{\text{eq}}(f)), \quad (2.3)$$

where τ is the relaxation time, and f_i^{eq} is the local equilibrium (Ansumali *et al.* 2003):

$$f_i^{\text{eq}} = \rho W_i \left(2 - \sqrt{1 + 3u_x^2}\right) \left(2 - \sqrt{1 + 3u_y^2}\right) \left(\frac{2u_x + \sqrt{1 + 3u_x^2}}{1 - u_x}\right)^{c_{xi}} \left(\frac{2u_y + \sqrt{1 + 3u_y^2}}{1 - u_y}\right)^{c_{yi}}, \quad (2.4)$$

where $u_\alpha = j_\alpha/\rho$, and the speed of sound is $c_s = 1/\sqrt{3}$. The local equilibrium distribution f_i^{eq} is the minimizer of the discrete H function (Karlin *et al.* 1999; Ansumali *et al.* 2003):

$$H = \sum_{i=1}^9 f_i \ln \left(\frac{f_i}{W_i}\right), \quad \text{with weights } W = \left[\frac{16}{36}, \frac{4}{36}, \frac{4}{36}, \frac{4}{36}, \frac{4}{36}, \frac{1}{36}, \frac{1}{36}, \frac{1}{36}, \frac{1}{36}\right], \quad (2.5)$$

under the constraints of the local hydrodynamic fields (2.2). Note the important factorization over spatial components of the equilibrium (2.4). This is similar to the familiar property of the local Maxwell distribution, and it distinguishes (2.4) among other discrete-velocity equilibria.

In the hydrodynamic regime, the model recovers the Navier-Stokes equation with viscosity coefficient $\mu = p\tau$, where $p = \rho c_s^2$ is the pressure (see section 5). The diffusive-wall approximation (Ansumali & Karlin 2002b) is used for wall boundary conditions.

3. Grad's moment system and the minimal kinetic model

3.1. The moment system

It is useful to represent the discrete velocity model (2.3) in the form of a moment system. For simplicity, we shall consider the linearized version of the model. Note that linearization is required only for the collision term on the right hand side of equation (2.3). This is at variance with Grad's moment systems (Grad 1949) where the advection terms are nonlinear as well. We choose the following nine non-dimensional moments as independent variables:

$$M = \left[\frac{\rho}{\rho_0}, \frac{j_x}{\rho_0 c_s}, \frac{j_y}{\rho_0 c_s}, \frac{P}{\rho_0 c_s^2}, \frac{N}{\rho_0 c_s^2}, \frac{P_{xy}}{\rho_0 c_s^2}, \frac{q_x}{2\rho_0 c_s^3}, \frac{q_y}{2\rho_0 c_s^3}, \frac{\psi}{2\rho_0 c_s^4} \right], \quad (3.1)$$

where

$$\psi = R_{yyyy} + R_{xxxx} - 2R_{xyxy}, \quad (3.2)$$

is a scalar obtained from 4th-order moments $R_{\alpha\beta\gamma\theta} = \sum_{i=1}^9 f_i c_{\alpha i} c_{\beta i} c_{\gamma i} c_{\theta i}$, $N = \sum_{i=1}^9 f_i (c_{xi}^2 - c_{yi}^2)/2 \equiv (P_{xx} - P_{yy})/2$ is the difference of the normal stresses, $P = \sum_{i=1}^9 f_i c_i^2$ is the trace of the pressure tensor, and $q_\alpha = \sum_{i=1}^9 f_i c_{\alpha i} c_i^2$ is the energy flux obtained by contraction of the third-order moment $Q_{\alpha\beta\gamma} = \sum_{i=1}^9 f_i c_{\alpha i} c_{\beta i} c_{\gamma i}$. Time and space are made non-dimensional in such a way that for a fixed system size L they are measured in the units of mean free time and mean free path, respectively: $\mathbf{x}' = \mathbf{x}/(L\text{Kn})$, $t' = t/\tau$, where $\text{Kn} = \tau c_s/L$ is the Knudsen number. The linearized equations for the moments M (3.1) read (from now on we use the same notation for the non-dimensional variables):

$$\begin{aligned} \partial_t \rho + \partial_x j_x + \partial_y j_y &= 0, \\ \partial_t j_x + \partial_x (P + N) + \partial_y P_{xy} &= 0, \\ \partial_t j_y + \partial_x P_{xy} + \partial_y (P - N) &= 0, \\ \partial_t P + \partial_x q_x + \partial_y q_y &= (\rho - P), \\ \partial_t N + \partial_x (q_x - Q_{xyy}) - \partial_y (q_y - Q_{yxx}) &= -N, \\ \partial_t P_{xy} + \partial_x Q_{yxx} + \partial_y Q_{yyx} &= -P_{xy}, \\ \partial_t q_x + \partial_x R_{xx\alpha\alpha} + \partial_y R_{xy\alpha\alpha} &= (2j_x - q_x), \\ \partial_t q_y + \partial_x R_{xy\alpha\alpha} + \partial_y R_{yy\alpha\alpha} &= (2j_y - q_y), \\ \partial_t \psi + \partial_x (j_x - q_x) + \partial_y (j_y - q_y) &= (2\rho - \psi). \end{aligned} \quad (3.3)$$

Furthermore, by construction of the discrete velocities (2.1), the following relations are satisfied:

$$\begin{aligned} Q_{xyy} &= 2q_x - 3j_x, & Q_{yxx} &= 2q_y - 3j_y, & (3.4) \\ R_{xy\alpha\alpha} &= 3P_{xy}, & R_{xx\alpha\alpha} &= 3\left(P + \frac{1}{2}N\right) - \frac{1}{2}\psi, & R_{yy\alpha\alpha} &= 3\left(P - \frac{1}{2}N\right) - \frac{1}{2}\psi. & (3.5) \end{aligned}$$

Apart from the lack of conservation of the energy and linearity of the advection, equation (3.3) is quite similar to Grad's two-dimensional 8-moment system †. However, in the present case a particular component of the 4th-order moment is also included as a variable. In other words, Grad's non-linear closure for the 4th-order moment is replaced by

† The variables used in the D -dimensional Grad's system are density, D components of the momentum flux, $D(D+1)/2$ components of the pressure tensor and D components of the energy flux. The number of fields in Grad's system is 8 for $D = 2$ and 13 for $D = 3$.

an evolution equation with a linear advection term. We note here that while the formulation of boundary conditions for Grad's moment system remains an open problem, the boundary conditions for the extended moment system (system 3.3, 3.4, and 3.5) are well established through its discrete-velocity representation (2.3) (Ansumali & Karlin 2002*b*). We also note that like any other Grad's system the present model reproduces the Navier-Stokes equation in the hydrodynamic limit (Karlin *et al.* 1999; Ansumali *et al.* 2003). The moment system (3.3) reveals the meaning of the densities appearing in model: The dimensionless density is the dimensionless pressure of the real fluid in the low Mach number limit, while the momentum flux density should be identified with the velocity in the incompressible limit. With this identification, we shall compare the moment system (3.3) with Grad's system.

3.2. One-dimensional Grad's moment system

Since energy is not conserved by the model (2.3), the comparison will be with another Grad moment system which (for $D = 3$) is usually referred to as the 10-moment system †. For one-dimensional flows, the linearized Grad's 10-moment system can be written as (Gorban & Karlin 2005; Karlin & Gorban 2002):

$$\partial_t p + \gamma \partial_x u_x = 0, \quad \partial_t u_x + \partial_x P_{xx} = 0, \quad \partial_t P_{xx} + 3 \partial_x u_x = -(P_{xx} - p), \quad (3.6)$$

where γ is the ratio of the specific heats of the fluid, and $\gamma = (D + 2)/D$ for a D -dimensional dilute gas. This model can be described in terms of its dispersion relation, which upon substitution of the solution in the form $\sim \exp(\omega t + ikx)$ reads:

$$\omega^3 + \omega^2 + 3k^2\omega + \gamma k^2 = 0. \quad (3.7)$$

The low wave-number asymptotic represents the large-scale dynamics (hydrodynamic scale of $\text{Kn} \ll 1$), while the high-wave number limit represent the molecular scales quantified by $\text{Kn} \gg 1$. The low wave number ($\text{Kn} \ll 1$) asymptotic, ω_l , and the large wave number ($\text{Kn} \gg 1$) asymptotic, ω_h , are:

$$\omega_l = \left\{ \frac{(-3 + \gamma)}{2} k^2 \pm i\sqrt{\gamma}k, -1 - (-3 + \gamma)k^2 \right\}, \quad \omega_h = \left\{ \frac{(-3 + \gamma)}{6} \pm i\sqrt{3}k, -\frac{\gamma}{3} \right\}. \quad (3.8)$$

The two complex conjugate modes (acoustic modes) of the $O(k^2)$ dynamics, are given by the first two roots of ω_l , and represent the hydrodynamic limit (the Navier-Stokes approximation) of the model. The third root in this limit is real and negative, corresponding to the relaxational behavior of the non-hydrodynamic variable (stress): the dominant contribution (equal to -1) is the relaxation rate towards the equilibrium value, while the next-order correction suggests slaving of viscous forces, which amounts to the constitutive relation for stress $((-3 + \gamma)/2k^2)$. Furthermore, the k^2 dependence of the relaxation term justifies the assumption of scale separation (the higher the wave-number, the faster the relaxation). The real part of the high wave-number solution ω_h is independent of k , which shows that the relaxation at very high Knudsen number is the same for all wavenumbers (so-called ‘‘Rosenau saturation’’ (Gorban & Karlin 1996; Slemrod 1998)). Thus, the assumption of scale-separation is not valid for high Knudsen number dynamics.

† The variables used in this D -dimensional Grad's system are density, D components of the momentum flux, and $D(D + 1)/2$ components of the pressure tensor, resulting in 6 and 10 variables for $D = 2$ and $D = 3$, respectively.

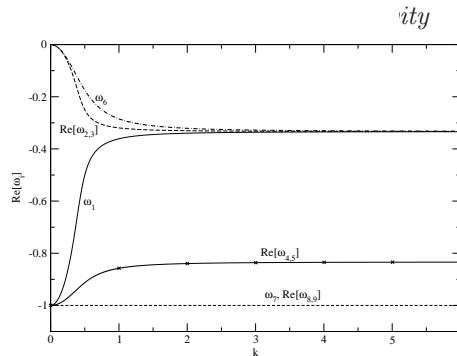


FIGURE 1. Real part of the solutions of the dispersion relation (equation (3.9)). Roots $\omega_{2,3}$ and ω_1 correspond to Grad’s subsystem (equation (3.6)). The real-valued root ω_6 and the complex conjugate roots $\omega_{2,3}$ are extended hydrodynamic modes.

3.3. Dispersion relation for the moment system

The dispersion relation for the one-dimensional version of the moment system (3.3) (i.e. neglecting all derivatives in the y -direction) reads:

$$(\omega^3 + \omega^2 + 3k^2\omega + k^2)(\omega^3 + 2\omega^2 + (3k^2 + 1)\omega + k^2)(1 + \omega)((1 + \omega^2) + 2k^2) = 0. \quad (3.9)$$

The real parts of the roots of this equation (attenuation rates $\text{Re}[\omega(k)]$) are plotted in Fig. 1 as functions of the wave vector k . It is clear that for one-dimensional flows, the dynamics of three of the moments (ρ , j_x , and P) are decoupled from the rest of the variables, and follows of the dynamics of the one-dimensional Grad’s moment system (3.6) with $\gamma = 1$.

The similarity between Grad’s moment system and the present model is an important fingerprint of the kinetic nature of the latter †. Note that in the case of two-dimensional flows, the agreement between the present model and Grad’s system is only qualitative. The present moment system is isotropic only up to $O(k^2)$. Thus, the dispersion relation of the model (2.3) is expected to match the one of Grad’s system only up to the same order. In the hydrodynamic and slip-flow regime addressed below, this order of isotropy is sufficient. In the presence of boundaries and/or non-linearities, it is necessary to resort to numerics. Below we use the entropic lattice Boltzmann discretization method (ELBM) of the model (2.3).

4. Flow in a lid-driven micro-cavity

The two-dimensional flow in a lid-driven cavity was simulated with ELBM over a range of Knudsen numbers defined as $\text{Kn} = \text{Ma}/\text{Re}$. In the simulations, the Mach number was fixed at $\text{Ma} = 0.01$ and the Reynolds number, Re , was varied. Initially, the fluid in the cavity is at rest and the upper wall of the domain is impulsively set to motion with $u_{\text{lid}} = c_s \text{Ma}$. Diffusive boundary conditions are imposed at the walls (Ansumali & Karlin 2002b), and the domain was discretized using 151 points in each spatial direction. Time

† Grad (Grad 1949) already mentioned that moment systems are particularly well suited for low Mach number flows. Qualitatively, this is explained as follows: when expansion in the Mach number around the no-flow state is addressed, the first nonlinear terms in the advection are of order $u^2/c_s^2 \sim \text{Ma}^2$. On the other hand, the same order in Ma terms in the relaxation contribute $u^2/(\tau c_s^2) \sim \text{Ma}^2/\text{Kn}$. Thus, if Knudsen number is also small, nonlinear terms in the advection can be neglected while the nonlinearity in the relaxation should be kept. That is why the model (2.3) - linear in the advection and nonlinear in the relaxation - belongs to the same domain of validity as Grad’s moment systems for subsonic flows.

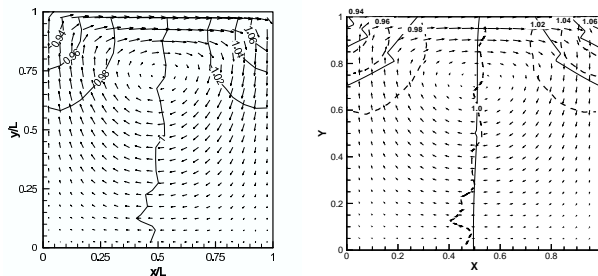


FIGURE 2. Flow in a micro-cavity for $\text{Kn} = 0.1$ and $\text{Ma} = 0.14$: DSMC simulation (Jiang *et al.* 2003) (left) , velocity vector plot and density isolines from ELBM (solid lines) with the DSMC density isolines (dashed lines) superimposed (right).

integration is continued till the steady state is reached; matrix-free, Newton-Krylov fixed point algorithms for the accelerated computation of the steady state are also being explored (Theodoropoulos *et al.* 2000).

4.1. Validation with DSMC simulation of the micro-cavity

In the hydrodynamic regime, the model was validated using results available from continuum simulations (Ansumali & Karlin 2002a). For higher $\text{Kn} \sim 0.1$, we compared our results with the DSMC simulation of (Jiang *et al.* 2003). Good agreement between the DSMC simulation and the ELBM results can be seen in Fig. 2. It can be concluded, that even for finite Knudsen number, the present model provides semi-quantitative agreement, as far as the flow profile is concerned. We remind here again, that the dimensionless density in the present model corresponds to the dimensionless pressure of a real fluid so that, for quantitative comparison, the density of ELBM model should be compared with the pressure computed from DSMC.

4.2. Parametric study of the flow in the micro-cavity

Fig. 3 shows the dimensionless density profiles with the streamlines superimposed for $\text{Kn} = 0.001, 0.01, 0.1$. For $\text{Kn} = 0.001$ ($\text{Re} = 10$), the behavior expected from continuum simulations with a large central vortex and two smaller recirculation zones close to the lower corners can be observed. As the Knudsen number is increased, the lower corner vortices shrink and eventually disappear and the streamlines tend to align themselves with the walls.

The density profiles, as a function of Kn , demonstrate that the assumption of incompressibility is well justified only in the continuum regime, where the density is essentially constant away from the corners. This observation is consistent with the conjecture that incompressibility requires smallness of the Mach as well as of the Knudsen number. In hydrodynamic theory, the density waves decay exponentially fast (with the rate of relaxation proportional to Kn) leading effectively to incompressibility. Thus, it is expected that the onset of incompressibility will be delayed as the Knudsen number increases.

5. Reduced description of the flow

The data from the direct simulation of the present kinetic model were used to validate the effectiveness of different closure approximations of kinetic theory in the presence of kinetic boundary layers in a fairly non-trivial flow, and to gain some insight about the

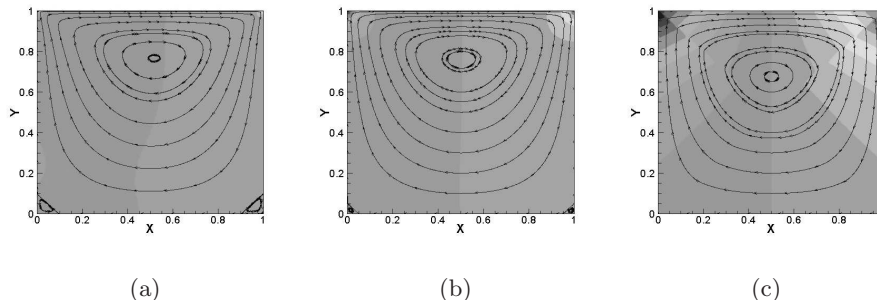


FIGURE 3. Density isocontours for (a) $\text{Kn} = 0.001$, (b) $\text{Kn} = 0.01$, and (c) $\text{Kn} = 0.1$ (the variation of the density is $0.995 \leq \rho \leq 1.005$). Superimposed are the streamlines.

required modification of the closure approximations in the presence of boundary layers. In this section, we will present such an analysis for two widely used closure methods, the Navier-Stokes approximation of the Chapman-Enskog expansion and Grad's moment closure.

5.1. The Navier-Stokes approximation

The Chapman-Enskog analysis (Chapman & Cowling 1970) of the model kinetic equation leads to a closure relation for the non-equilibrium part of the pressure tensor as (the Navier-Stokes approximation):

$$\sigma_{xy} = -\tau c_s^2 (\partial_y j_x + \partial_x j_y). \quad (5.1)$$

Fig. 4 shows a scatter plot of the xy component of the non-equilibrium part of the pressure tensor $P_{xy} - P_{xy}^{\text{eq}}$, versus that computed from the Navier-Stokes approximation of the Chapman-Enskog expansion (5.1). The upper row is the scatter plot for all points in the computational domain, while the lower row is the scatter plot obtained after removal of the boundary layers close to the four walls of the cavity, corresponding to approximately 10 mean-free paths. In all plots, the dashed straight line of slope equal to one corresponds to Navier-Stokes behavior. These plots clearly reveal that the Navier-Stokes description is valid away from the walls in the continuum as well as in the slip flow regime. On the other hand, it fails to represent hydrodynamics in the kinetic boundary layer.

Perhaps the most interesting observation from Fig. 4 is the coherent, curve-like structure of the off-Navier-Stokes points. These trajectories tend to the Navier-Stokes approximation as to an attractive sub-manifold. This structure resembles the trajectories of solutions to the invariance equation (Gorban & Karlin 2005; Gorban *et al.* 2004) observed, in particular, in a similar problem of derivation of hydrodynamics from Grad's systems (see, e. g. Karlin & Gorban (2002), p. 831, Fig. 12). A link between solutions to invariance equations and the present simulations is an intriguing subject for further study. In the next subsection, we shall explore Grad's closure approximation for the present flow.

5.2. Grad's approximation

In contrast to the Chapman-Enskog method, the Grad method has an advantage that the approximations are local in space, albeit with an increased number of fields. As the analysis of section 3 suggests, the dynamics of the density, momentum and pressure tensor

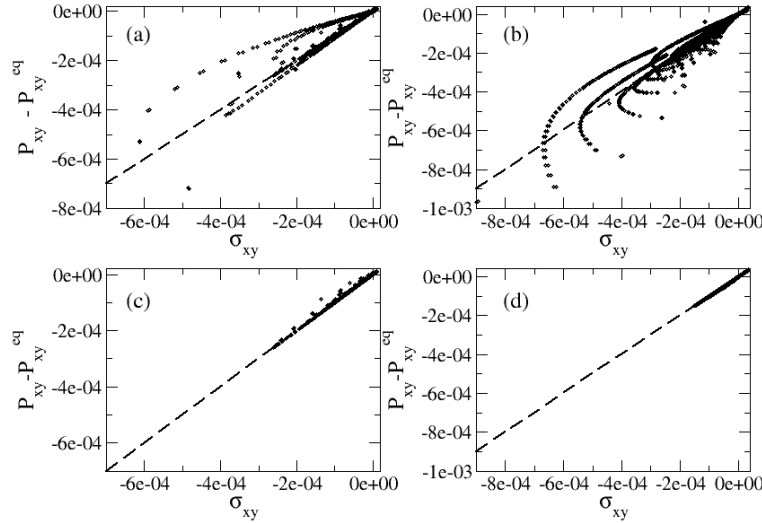


FIGURE 4. Scatter plot of the non-equilibrium part of the off-diagonal component of the pressure tensor $P_{xy} - P_{xy}^{\text{eq}}$ and corresponding value computed from Navier-Stokes approximation σ_{xy} (5.1) for all points in the domain ((a) and (b)), and after the removal of the boundary layer corresponding to approximately 10 mean-free path ((c) and (d)). Fig. (a,c) correspond to $\text{Kn} = 0.001$, while Fig. (b,d) correspond to $\text{Kn} = 0.01$. Navier-Stokes behavior is indicated by the straight line of slope equal to one.

are almost decoupled from the rest of the moments, at least away from boundaries. This motivates the Grad-like approximation for the populations,

$$f_i^{\text{Grad}} = W_i \left[\rho + \frac{j_\alpha c_{i\alpha}}{c_s^2} + \frac{1}{2c_s^4} (P_{\alpha\beta} - \delta_{\alpha\beta} \rho c_s^2) (c_{i\alpha} c_{i\beta} - c_s^2 \delta_{\alpha\beta}) \right]. \quad (5.2)$$

The set of populations parameterized by the values of the density, momentum and pressure tensor (5.2) is a sub-manifold in the phase space of the system (2.3), and can be derived in a standard way using quasi-equilibrium procedures (Gorban & Karlin 2005; Gorban *et al.* 2004). After taking into account the time discretization, we find the closure relation for the energy flux:

$$q_\alpha^{\text{Grad}} = \frac{4}{3} \left(1 + \frac{p}{2\mu} \right) j_\alpha - \frac{p}{2\mu} q_\alpha^{\text{eq}}. \quad (5.3)$$

In Fig. 5, the scatter plot of the computed energy flux q_x and the discrete Grad's closure q_x^{Grad} (5.3) is presented. Same as in Fig. 4, the off-closure points in Fig. 5 are associated with the boundary layers. The comparison of the quality with which the closure relations are fulfilled in Fig. 4 and Fig. 5 clearly indicates the advantage of that a Grad's closure. Various strategies of a domain decomposition for a reduced simulation can be devised based on this observation. A general conclusion is that for slow flows Grad's closure in the bulk along with the discretization of the boundary condition (Ansumali & Karlin 2002b) is the optimal strategy for the simulation of microflows.

6. Conclusions and further studies

We considered a specific example of a minimal kinetic model for studies of microflows, and compared it with other theories of nonequilibrium thermodynamics in a nontriv-

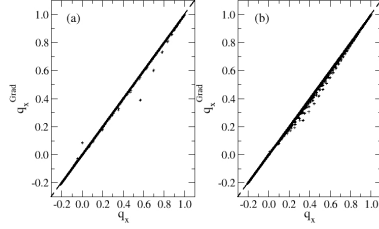


FIGURE 5. Scatter plot of the computed energy flux, q_x , versus Grad's closure, q_x^{Grad} : (a) $\text{Kn} = 0.001$, (b) $\text{Kn} = 0.01$.

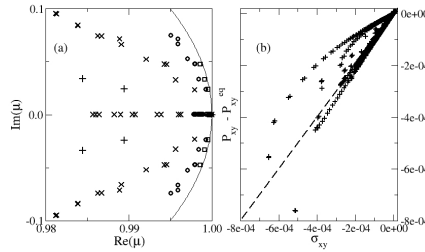


FIGURE 6. (a) Leading eigenvalues of the minimal kinetic model at steady state (square: $\text{Kn}=10^{-4}$, circle: $\text{Kn}=10^{-3}$, X: $\text{Kn}=10^{-2}$, +: $\text{Kn}=10^{-1}$); (b) Scatter plot as in Fig. 4(a) for a state perturbed away from the steady state along the leading eigenvector ($\text{Kn}=10^{-3}$).

ial flow situation. The close relationship between Grad's moment systems and minimal kinetic models was highlighted. For the case of a driven cavity flow, different closure approximations were tested against the direct simulation data, clearly showing the failure of the closures near the boundaries. Grad's closure for the minimal model was found to perform better than the Navier-Stokes approximation. This finding can be used to reduce the memory requirement in simulations, while preserving the advantage of locality.

In this paper, we have explored two classical closures of kinetic theory. In the future we are going to consider other closures such as the invariance correction to Grad's closure, and especially closures based on spectral decomposition (Gorban & Karlin 2005). To that end, the ELBM code was coupled with ARPACK (Lehoucq *et al.* 1998) in order to compute the leading eigenvalues and the corresponding eigenvectors of the Jacobian field of the corresponding map at the steady state. In all cases, the eigenvalues are within the unit circle (Fig. 6(a)). The leading eigenvalue is always equal to one (reflecting mass conservation), and the corresponding eigenvector captures most of the structure of the steady state. As the Knudsen number decreases, eigenvalues tend to get clustered close to the unit circle. This happens because when the Knudsen number is small the incompressibility assumption is a good approximation, and mass is also conserved locally. The very close similarity between fig. 6(b) and fig. 4(a), reveals that states perturbed away from the steady state along the leading eigenvector are also described well by the Navier-Stokes closure.

Acknowledgement. Discussions with A. N. Gorban are gratefully acknowledged. The work of SA, CEF and IVK was partially supported by the Swiss Federal Department of Energy (BFE) under the project Nr. 100862 "Lattice Boltzmann simulations for chemi-

cally reactive systems in a micrometer domain”. The work of IGK was partially supported by an NSF-ITR grant and by DOE.

REFERENCES

- ANSUMALI, S. & KARLIN, I. V. 2002*a* Entropy Function Approach to the Lattice Boltzmann Method. *J. Stat. Phys.* **107**(1-2), 291–308.
- ANSUMALI, S. & KARLIN, I. V. 2002*b* Kinetic Boundary Condition for the Lattice Boltzmann Method. *Phys. Rev. E* **66**(2), 026311.
- ANSUMALI, S., KARLIN, I. V., FROUZAKIS, C. E. & BOULOUCHOS, K. B. 2004 Entropic Lattice Boltzmann Method for Microflows. <http://xxx.lanl.gov/abs/cond-mat/0412555> .
- ANSUMALI, S., KARLIN, I. V. & ÖTTINGER, H. C. 2003 Minimal Entropic Kinetic Models for Simulating Hydrodynamics. *Europhys. Lett.* **63**(6), 798–804.
- BESKOK, A. & KARNIADAKIS, G. E. 2001 *Microflows: Fundamentals and Simulation*. Springer, Berlin.
- BIRD, G. A. 1994 *Molecular Gas Dynamics and the Direct Simulation of Gas Flows. Theory and Application of the Boltzmann Equation*. Oxford University Press.
- CERCIGNANI, C. 1975 *Theory and Application of the Boltzmann Equation*. Scottish Academic Press, Edinburgh.
- CHAPMAN, S. & COWLING, T. G. 1970 *The Mathematical Theory of Non-Uniform Gases*. Cambridge University Press, Cambridge.
- GORBAN, A. N. & KARLIN, I. V. 1996 Short-wave Limit of Hydrodynamics: A Soluble Example. *Phys. Rev. Lett.* **77**, 282–285.
- GORBAN, A. N. & KARLIN, I. V. 2005 *Invariant Manifolds for Physical and Chemical Kinetics*. Springer, Berlin Heidelberg.
- GORBAN, A. N., KARLIN, I. V. & ZINOVYEV, A. Y. 2004 Constructive Methods of Invariant Manifolds for Kinetic Problems. *Phys. Rep.* **396**, 197–403.
- GRAD, H. 1949 On the Kinetic Theory of Rarefied Gases. *Comm. Pure Appl. Math.* **2**, 331–407.
- JIANG, J.-Z., JI, F. & SHEN, C. 2003 Statistical simulation of micro-cavity flows. *23rd Int. Symposium on Rarefied Gas Dynamics* pp. 784–790.
- KARLIN, I. V., FERRANTE, A. & ÖTTINGER, H. C. 1999 Perfect Entropy Functions of the Lattice Boltzmann Method. *Europhys. Lett.* **47**, 182–188.
- KARLIN, I. V. & GORBAN, A. N. 2002 Hydrodynamics from Grad’s Equations: What can We Learn from Exact Solutions? *Ann. Phys. (Leipzig)* **11**, 783–833.
- KEVREKIDIS, I. G., GEAR, C., HYMAN, J. M., KEVREKIDIS, P. G., RUNBORG, O. & THEODOROPOULOS, C. 2003 Equation-free, Coarse-grained Multiscale Computation: Enabling Microscopic Simulators to Perform System -level Analysis. *Comm. Math. Sci.* **1**, 715–762.
- KEVREKIDIS, I. G., GEAR, C. W. & HUMMER, G. 2004 Equation-free: the Computer-assisted Analysis of Complex, Multiscale systems. *A. I. Ch. E. Journal* **50** (7), 1346–1354.
- LEHOUCQ, R., SORENSEN, D. & YANG, C. 1998 *ARPACK Users’ Guide: Solution of Large-Scale Eigenvalue Problems with Implicitly Restarted Arnoldi Methods*. SIAM.
- NIU, X. D., SHU, C. & CHEW, Y. 2003 Lattice Boltzmann BGK Model for Simulation of Micro Flows. *Euro. Phys. Lett.* **67**, 600–606.
- ORAN, E. S., OH, C. K. & CYBYK, B. Z. 1998 Direct Simulation Monte Carlo: Recent Advances and Applications. *Annu Rev. Fluid Mech.* **30**, 403–441.
- SLEMRD, M. 1998 Renormalization of the Chapman-Enskog Expansion: Isothermal Fluid Flow and Rosenau Saturation. *J. Stat. Phys.* **91**, 285–305.
- SUCCI, S. & SBRAGAGLIA, M. 2004 Analytical Calculation of Slip Flow in Lattice Boltzmann Models with Kinetic Boundary Conditions. <http://arxiv.org/abs/nlin.CG/0410039> .
- THEODOROPOULOS, K., QIAN, Y.-H. & KEVREKIDIS, I. G. 2000 “Coarse” Stability and Bifurcation Analysis Using Timesteppers: a reaction diffusion example. *Proc. Natl. Acad. Sci.* **97** (18), 9840–9843.
- THEODOROPOULOS, K., SANKARANARAYANAN, K., SUNDARESAN, S. & KEVREKIDIS, I. G. 2004 Coarse Bifurcation Studies of Bubble Flow Lattice Boltzmann Simulations. *Chem. Eng. Sci.* **59**, 2357–2362.

ZHENG, Y., GARCIA, A. L. & ALDER, B. J. 2002 Comparison of Kinetic Theory and Hydrodynamics for Poiseuille Flow. *J. Stat. Phys.* **109**, 495–505.